THE ASTROPHYSICAL JOURNAL, 562:446–455, 2001 November 20

X-RAYS AND PROTOSTARS IN THE TRIFID NEBULA

JEONGHEE RHO
Infrared Processing and Analysis Center, California Institute of Technology, MS 100-22, Pasadena, CA 91125; rho@ipac.caltech.edu
MICHAEL F. CORCORAN
NASA Goddard Space Flight Center, Code 662, Greenbelt, MD 20742
YOU-HUA CHU
Department of Astronomy, University of Illinois, 1002 West Green Street, Urbana, IL 61801
AND
WILLIAM T. REACH
Space Infrared Telescope Facility Center, California Institute of Technology, MS 100-22, Pasadena, CA 91125
Received 2001 February 19; accepted 2001 June 28

ABSTRACT

The Trifid Nebula is a young H II region, recently rediscovered as a "pre-Orion" star-forming region, containing protostars undergoing violent mass ejections visible in optical jets as seen in images from the *Infrared Space Observatory* and the *Hubble Space Telescope*. We report the first X-ray observations of the Trifid Nebula using *ROSAT* and *ASCA*. The *ROSAT* image shows a dozen X-ray sources, with the brightest X-ray source being the O7 star, HD 164492, which provides most of the ionization in the nebula. We also identify 85 T Tauri star and young, massive star candidates from near-infrared colors using the JHK_s color-color diagram from the Two-Micron All-Sky Survey (2MASS). Ten X-ray sources have counterpart near-infrared sources. The 2MASS stars and X-ray sources suggest there are potentially numerous protostars in the young H II region of the Trifid. *ASCA* moderate-resolution spectroscopy of the brightest source shows hard emission up to 10 keV with a clearly detected Fe K line. The best model fit is a two-temperature ($T = 1.2 \times 10^6$ K and 39×10^6 K) thermal model with additional warm absorbing media. The hotter component has an unusually high temperature for either an O star or an H II region; a typical Galactic H II region could not be the primary source for such hot temperature plasma and the Fe XXV line emission. We suggest that the hotter component originates in either the interaction of the wind with another object (a companion star or a dense region of the nebula) or from flares from deeply embedded young stars.

Subject headings: H II regions — infrared: stars — stars: formation — X-rays: individual (Trifid Nebula)

1. INTRODUCTION

H II regions contain various types of X-ray–emitting sources, such as high- and low-mass stars, binaries, and protostars. Single massive O and B stars emit soft X-rays from shocks in their radiatively unstable, outwardly moving outer atmospheres. X-ray emission from late-type stars is attributed to magnetically heated stellar coronae and magnetically driven stellar flares. Protostars produce X-rays via magnetic heating and perhaps from accretion or excretion disks and/or interaction of stellar jets with the circumnebular gas. Massive binaries can produce X-ray emission from colliding stellar winds; close low-mass binaries can produce X-rays via mass exchange and enhanced dynamo action. X-ray emission provides a sensitive tracer of these different stellar populations and, along with infrared colors, is one of the main probes for identifying protostars and pre–main-sequence (PMS) stars.

Studies of X-ray emission from H II/star-forming regions have made significant advances because of *ROSAT* (Casanova et al. 1995), *ASCA* (e.g., Koyama et al. 1996), and, most recently, *Chandra* observations (Garmire et al. 2000). For example, in the ρ Oph core region, 70% of the near-infrared (NIR) sources associated with protostars and molecular cores have X-ray counterparts (Casanova et al. 1995), and a large number of X-ray sources have been found to be low-mass PMS stars in other star-forming regions such as Orion (Alcalá et al. 1996), Chamaeleon (Alcalá et al. 1995; Feigelson et al. 1993), Lupus (Krautter et al. 1997), and Taurus-Auriga (Neuhüser et al. 1995; Wichmann et al. 1997). Flarelike X-ray events have been detected from T Tauri stars (Kamata et al. 1997; Koyama et al. 1992). The X-ray–emitting sources in the Monoceros and Rosette molecular clouds are also mostly T Tauri and Herbig Ae/Be stars and they typically show luminosities of $L_X \sim 10^{30}$–10^{32} ergs s^{-1} (Gregorio-Hetem et al. 1998). Recent *Chandra* observation of the Orion Nebula resolved a thousand X-ray–emitting PMS stars with a mass range of 0.05 to 50 $M_\odot$, and a combined infrared and X-ray study suggested that the X-ray luminosity depends on stellar mass, rotational history, and magnetic field (Garmire et al. 2000).

At a distance of 1.67 kpc (Lynds & O'Neil 1985), the Trifid Nebula, M20, is one of the best-known astrophysical objects and one of the prettiest: it glows brightly in red light and is trisected by obscuring dust lanes. At an age of $\sim 3 \times 10^5$ yr, the Trifid is one of the youngest known H II regions. Observations with the *Infrared Space Observatory* (*ISO*) and the *Hubble Space Telescope* (*HST*) show the Trifid as a dynamic, "pre-Orion" star-forming region containing young stars undergoing episodes of violent mass ejections, and protostars (like HH 399) losing mass and energy to the nebula in optically bright jets (Cernicharo et al. 1998, hereafter CLC98; Lefloch & Cernicharo 2000; Hester et al. 1999). The ionization of the nebular gas is dominated by the O7.5 star HD 164492. HD 164492 is a

luminosity class V (Levato 1975) or III (Conti & Alschuler 1971) star with a bolometric luminosity of $L_{bol} \sim 0.5$–1.6×10^{39} ergs s^{-1} and an X-ray luminosity of 6×10^{32} ergs s^{-1} (Chlebowski et al. 1989). The mass-loss rate of this O star is $\dot{M} = 2 \times 10^{-6}\ M_{\odot}$ yr^{-1} (Howarth & Prinja 1989) and the wind terminal velocity is $V_{\infty} = 1580$ km s^{-1} (Prinja, Barlow, & Howarth 1990).

X-ray observations of the Trifid offer a unique opportunity to study the influence of a massive star on star formation in an exceptionally young star-forming region. Initially, X-ray emission from the Trifid was reported only from the O star in the *Einstein* IPC catalog (Chlebowski & Harnden 1989). We serendipitously discovered a complex of X-ray emission from the Trifid Nebula in a PSPC observation of the nearby supernova remnant W28 (Rho et al. 1995). Subsequently, we started an extensive investigation of the X-ray emission from the Trifid Nebula. This paper presents the first detection of a dozen X-ray sources in the Trifid Nebula, and we correlate these with protostar candidates identified using the Two-Micron All-Sky Survey (2MASS) data. The *ROSAT* images show multiple point sources, including HD 164492 and several T Tauri stars, and the *ASCA* spectra show hard X-ray emission, including detection of an Fe K line. We discuss identifications of the X-ray–emitting sources and the origin of the unusually hard X-ray emission from the Trifid.

2. X-RAY SOURCES IN THE TRIFID

2.1. *X-Ray Observations*

The Trifid Nebula was observed using the X-ray telescope on *ROSAT* (Trümper 1993) with the Position Sensitive Proportional Counter (PSPC) as the imaging detector. The PSPC on-axis angular resolution is 25″ (FWHM, at 1 keV), and the PSPC covers a 2° field of view in the 0.1–2.4 keV energy band. Two PSPC observations were analyzed for this paper: rp900375 centered on HD 164492 and observed on 1993 September 8 for an exposure of 9365 s (PI: S. Snowden), and rp500236 centered on the supernova remnant W28 and observed on 1993 April 1 for an exposure of 10,476 s (PI: R. Pisarski; Rho et al. 1995).

We also performed an *ASCA* observation (PI: J. Rho; sequence number 26051000) toward the center of the Trifid Nebula. The observation took place on 1998 September 30 to October 2. *ASCA* (TI & H94) has two detector pairs: Gas Imaging Spectrometers (GIS2 and GIS3) and Solid-State Imaging Spectrometers (SIS0 and SIS1). The SIS covers an energy band of 0.5–10 keV and the GIS 0.6–10 keV. The on-axis angular resolution of the GIS and SIS is about 1′–2′. Each GIS counter has a circular field of view of 35′ diameter while the field of view of each SIS CCD is an 11′ square; thus, both GIS and SIS detectors sufficiently cover the entire Trifid Nebula. We filtered the data using a few criteria such as cutoff rigidity (COR) and earth elevation (based on Revison 2 processing). After filtering, the exposure time was 57 ks for the GIS and 53.5 ks for the SIS. The entire Trifid Nebula region after background subtraction has count rates of 0.050 ± 0.001 counts s^{-1} for SIS0, 0.040 ± 0.001 counts s^{-1} for SIS1, 0.030 ± 0.008 counts s^{-1} for GIS2, 0.039 ± 0.009 counts s^{-1} for GIS3, and 0.086 ± 0.004 counts s^{-1} for the *ROSAT* PSPC, in their respective energy bands (integrated over all channels).

2.2. *X-Ray Source Identification*

The *ROSAT* PSPC image of the Trifid Nebula is shown in Figure 1. This image reveals for the first time that the Trifid Nebula contains numerous X-ray sources. We have identified X-ray sources in the PSPC image using the FTOOLS task SRCDETECT and estimated the count rates and uncertainties. The detected point sources are presented, in order of increasing right ascension, in Table 1 and marked in Figure 1. Table 1 lists the position, count rate, and σ of detection for 10 sources detected at greater than 3 σ and two possible sources (sources 11 and 12) detected with somewhat lower confidence. We define here new X-ray sources detected in the *ROSAT* PSPC image, as *ROSAT* X-ray source in the Trifid (RXT). Since the count rate is very small except for the O star HD 164492, we estimated the luminosity by assuming an absorption column density $N_{\rm H} = 3 \times 10^{21}$cm^{-2} ($A_V \sim 1.5^m$, see § 4 for details), and a thermal spectrum with $kT = 1$ keV. The X-ray emission of PMS stars is understood to be thermal emission from gas rapidly heated to a temperature of $\sim$1 keV by violent magnetohydrodynamic reconnection events (Feigelson & Montmerle 1999). The correspondence between the PSPC count rate and the X-ray unabsorbed flux is 1×10^{-3} PSPC counts s^{-1} $\sim 2.95 \times 10^{-14}$ ergs s^{-1} cm^{-2}. Using this conversion, the luminosities of the X-ray sources are computed and given in Table 1.

We have examined the source list database using SIMBAD, identified counterparts to the X-ray sources at other wavelengths, and marked them in Figure 1. To visualize the correspondence of X-ray sources with either optical or radio sources, we have plotted the X-ray contours over an Hα image (F. Winkler, 2001, private communication) in Figure 2. Twenty-four sources from the Guide Star Catalog (GSC) are visible in the Hα image in Figure 2. The brightest X-ray point source, RXT8 in Table 1, corresponds to the O star HD 164492. The possible X-ray source RXT11 coincides with the B8 star HD 313596 (R.A. $18^h02^m35^s$ and decl. $-22°59'54''$), and the possible X-ray source RXT12 with the

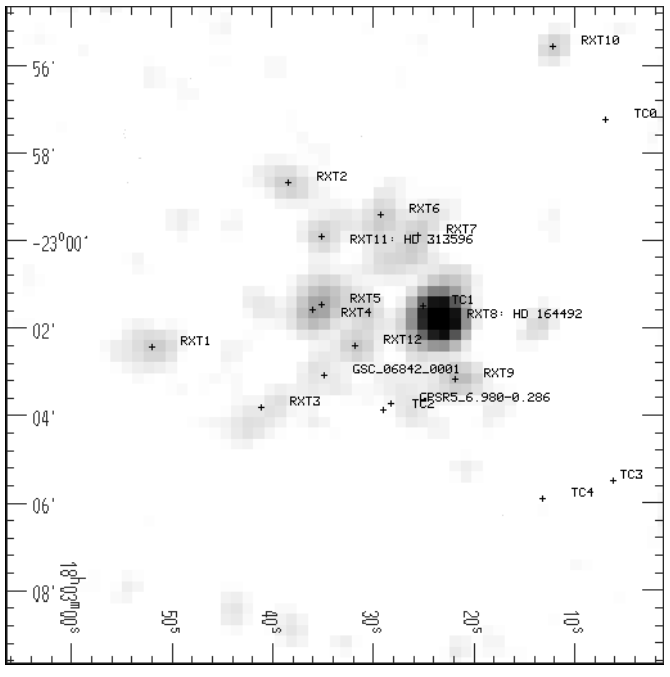

FIG. 1.—PSPC X-ray image and detected sources (RXT) are marked with numbers. Count rates for each source are listed in Table 1. Known sources are also marked with the labels.

TABLE 1

X-RAY SOURCES DETECTED IN THE PSPC IMAGE OF THE TRIFID NEBULA

Name	R.A. (2000)	Decl. (2000)	Count Rate	Detection (σ)	log (L_X)
RXT1	18 02 52.8	−23 02 18.1	0.0014 ± 0.0005	5	31.12
RXT2	18 02 39.3	−22 58 34.3	0.0011 ± 0.0004	3.5	31.02
RXT3	18 02 41.	−23 03 51.8	0.0014 ± 0.0006	3.5	31.12
RXT4	18 02 36.0	−23 01 36.3	0.0019 ± 0.0006	4	31.05
RXT5	18 02 35.0	−23 01 29.4	0.0021 ± 0.0006	4.5	31.29
RXT6	18 02 27.9	−22 59 47.9	0.0016 ± 0.0006	4	31.17
RXT7	18 02 25.4	−22 59 51.4	0.0010 ± 0.0005	3	30.97
RXT8	18 02 23.35	−23 01 47.0	0.0131 ± 0.0013	8	(see Table 4)
RXT9	18 02 21.1	−23 03 21.5	0.0010 ± 0.0004	4	30.97
RXT10.....	18 02 12.38	−22 55 37.0	0.0012 ± 0.0004	4.5	31.05
RXT11.....	18 02 34.92	−22 59 55.6	0.0006 ± 0.0003	2.5	30.75
RXT12.....	18 02 31.67	−23 02 25.6	0.0007 ± 0.0003	2.5	30.82

NOTE.—Units of right ascension are hours, minutes, and seconds, and units of declination are degrees, arcminutes, and arcseconds.

optical star GSC_06842_00001 (R.A. $18^h02^m34^s.8$ and decl. $-23°03'06''.3$). None of the other GSC stars coincide with X-ray peaks. A radio source, GPSR5 6.980−0.286 (R.A. $18^h02^m28^s.1$ and decl. $-23°03'46''.3$; Becker et al. 1994), is close to the X-ray–emitting area but does not have a corresponding X-ray peak. Four protostars (TC0, TC1, TC3, and TC4 sources[1] in CLC98) have been reported in the Trifid Nebula (CLC98), which are marked in Figure 1, but only one is close to the X-ray peak at HD 164492. In the next section, we correlate the PSPC X-ray sources with sources showing NIR color excesses and present candidate protostars.

[1] The source designation TC0, TC1, etc. was assigned by CLC98. Since this designation was already in use, for indexing purposes these sources should be referred to as [CLC98] 0, etc.

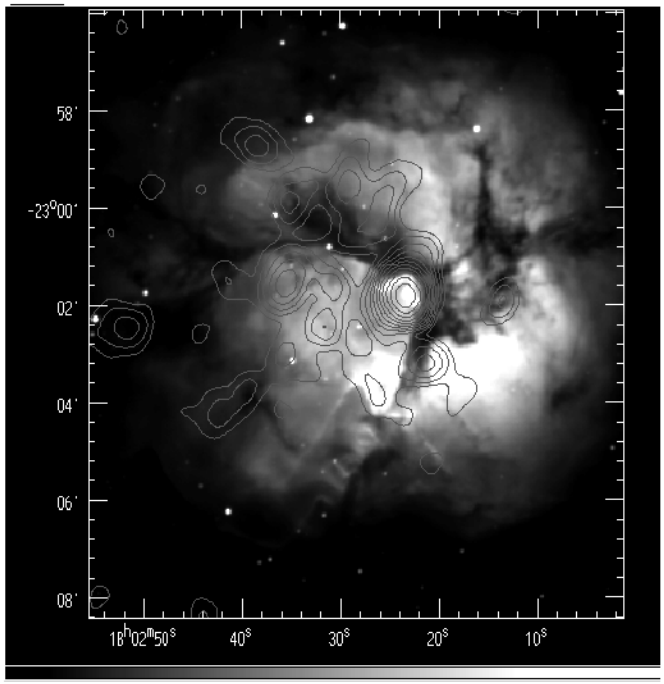

FIG. 2.—PSPC X-ray contours superimposed on an Hα image of the Trifid Nebula (courtesy of Frank Winkler). The optical image was obtained on 1994 July 4 (UT) from the Burrell Schmidt telescope of Case Western Reserve University through a 25 Å bandpass Hα filter. Total exposure time is 1800 s, and the scale is $2''.0$ pixel^{-1}. The strongest X-ray peak is at the O star, HD 164492.

3. NEAR-INFRARED SOURCES FROM 2MASS: YOUNG STELLAR OBJECTS

We have identified young stellar objects (YSOs) using the 2MASS data (Skrutskie et al. 1997). Using identical telescopes in the northern and southern hemispheres, 2MASS is mapping the entire sky in the J (1.11–1.36 μm), H (1.5–1.8 μm), and K_s (2–2.32 μm) bands to a limiting point-source sensitivity of approximately 16.5, 16.0, and 15.5 mag, respectively (Cutri et al. 2000).[2] The data toward the Trifid Nebula were taken on 1998 June 14 using the southern telescope, and most of these data were included in the 2MASS Second Incremental Release, but a small portion of area was in the 2MASS Working Database because of large photometric uncertainties at the time of the Incremental Release. The photometry is typically better than 5% (Cutri et al. 2000—see fn. 2).

We used the 2MASS point-source catalog to extract sources within an $8'$ radius centered on R.A. $18^h02^m30^s$ and decl. $-23°02'00''$. We have selected sources with the following criteria. First, we selected the sources that were detected in all three J, H, and K_s bands. We then selected sources with a signal-to-noise ratio greater than 10 (i.e., the J, H, and K_s magnitudes are brighter than 15.8, 15.1, and 14.3 mag, respectively). These selections produced ∼1100 such sources. We then accepted sources with photometric uncertainties $\sigma < 0.25$ mag, for which the fit to the point-spread function produced reduced $\chi^2_\nu < 2$. This last criterion excluded blended sources that caused higher uncertainties in the photometry. This is important in the Galactic plane where NIR sources are crowded and the 2MASS has a limited spatial resolution ($3''.5$). This criterion removed inaccurate blue points that appeared in the JHK_s color-color diagram (as described below). The criteria we have used are conservative for the magnitude limit and photometric uncertainties of the 2MASS survey.

We plotted the sources in the JHK_s color-color diagram, as shown in Figure 3*a*, in order to identify YSOs with infrared color excess. Figure 3*b* shows $H-K_s$ versus K_s magnitude for the selected sample. The interstellar reddening

[2] See R. M. Cutri et al. 2000, at http://www.ipac.caltech.edu/2mass/releases/ first/doc/explsup.html.

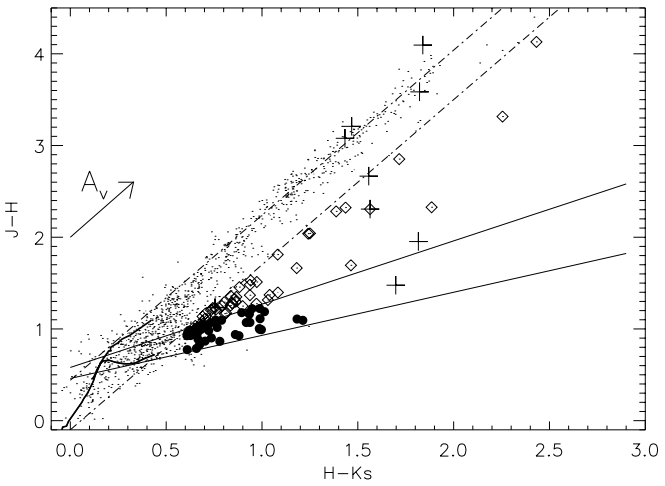

FIG. 3*a*

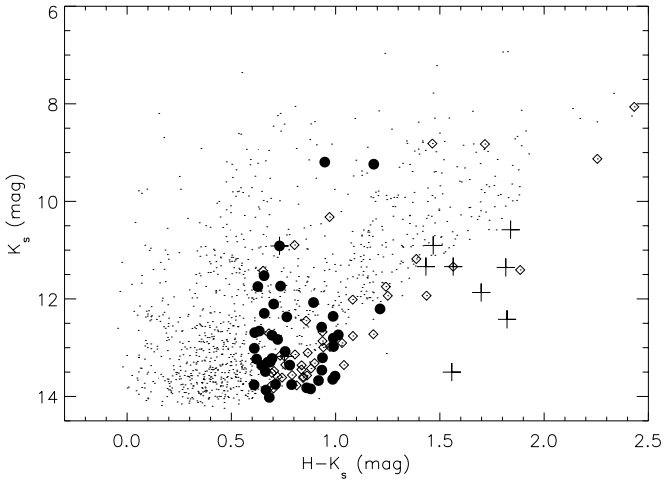

FIG. 3*b*

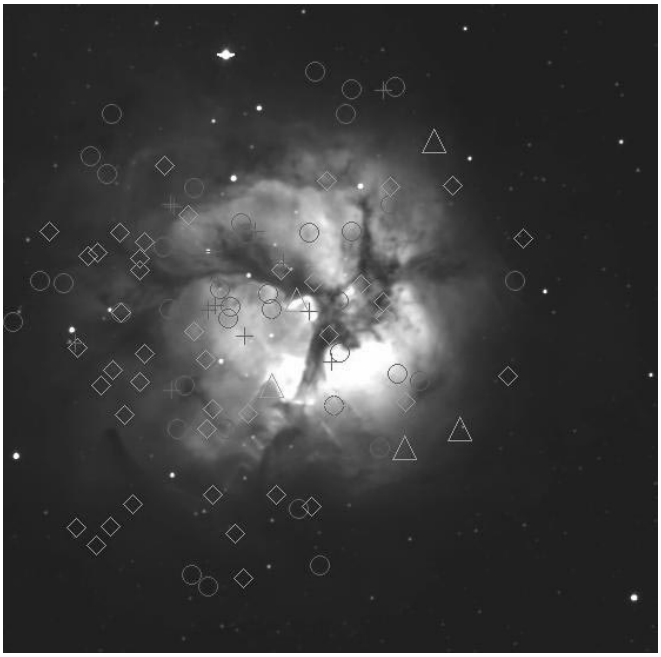

FIG. 3*c*

FIG. 3.—(*a*) Near-infrared JHK_s color-color diagram: location in color-color diagram is used to determine T Tauri stars and massive YSOs. Normal stars (*dots*), T Tauri stars (filled circles), and massive YSOs (*diamonds*) are shown with different symbols. The 2MASS counterparts of X-ray sources are marked with crosses; the sources above the extinction curve have high photometric uncertainties. They are 2MASS-red stars in Table 3 (see text for details). Extinction vector is shown for 5 mag as the thick line labeled A_v. Thick curves are intrinsic colors of giant and dwarf stars. (*b*) Diagram of $H - K_s$ vs. K_s. T Tauri stars and young massive protostars fall below (younger age) the PMS stars in this diagram. Symbols are the same as in (*a*). (*c*) T Tauri stars (*circles*) and massive YSOs (*diamonds*), X-ray sources (*crosses*), and known embedded YSOs (*triangles:* from Cernicharo et al. 1998) are marked on optical image. (*d*) 2MASS three-color image (blue, green, and red for J, H, and K_s, respectively). Symbols are the same as in (*c*). The diffuse, blue emission is probably Paβ (in the J band) from the H II region.

vector from Rieke & Lebofsky (1985) is also plotted. Adopting the intrinsic colors of giant and dwarf stars from Bessell & Brett (1988), we find the visual extinction toward this direction is as high as $A_V = 30$ mag for stars on the back side of the Trifid Nebula. The observed JHK_s colors of YSOs can be explained by circumstellar disk models (Lada & Adams 1992). We identified the T Tauri stars with $(J-H)_{\rm CTTS} = 0.58 \pm 0.11 \times (H-K_s)_{\rm CTTS} + 0.52 \pm 0.06$ (Meyer, Calvet, & Hillenbrand 1997) and $H-K_s > 0.6$ mag, where CTTS is classical T Tauri stars. These T Tauri stars fall between the two solid lines in Figure 3*a*. The stars below the extinction curve (*dashed line* in Fig. 3*a*) and above the T Tauri star lines (*solid line* in Fig. 3*a*) are massive YSOs (Lada & Adams 1992); these stars are plotted as diamonds in Figure 3*a*. In total, we found 41 T Tauri star candidates and 44 massive YSO candidates from the 2MASS sources that are listed in Table 2. The T Tauri stars and YSOs are generally located along the ionization front. Figure 3*c* shows optical images, and T Tauri stars, massive YSOs, and X-ray sources are marked. Figure 3*d* shows a color composite of the J, H, and K_s images, with the J image in blue, H image in green, and K_s image in red. T Tauri stars, massive

FIG. 3*d*

YSOs, and X-ray sources are marked. The image also shows a number of protostars at the ionization front along the dust lane.

These protostar candidates were cross-correlated with the X-ray sources. Taking into account the resolution of the PSPC, we identify a possible coincidence if the separation between a 2MASS source and an X-ray source is less than 15″. Three X-ray sources (RXT1, RXT6, and RXT7) are coincident with either T Tauri stars or YSOs; they are noted in Table 3. Figure 3*d* shows that many red 2MASS stars within the X-ray source error boxes could be considered coincidences, but they are not included in the list of sources selected according to the aforementioned conservative criteria as they are not detected in one or both of the J and H bands. Therefore, we have relaxed the selection criteria and extracted 2MASS sources from the same area, excluding only sources with an artifact flag. We made a list of the 2MASS sources that are within 15″ from X-ray sources. Each X-ray source has $\sim$10 2MASS counterpart candidates; only the red stars are identified as possible counterparts to the X-ray sources. Seven red 2MASS star counterparts of X-ray sources are identified and listed in Table 3, with J, H, and K_s magnitudes and reasons that they were not selected in the earlier list of T Tauri star or massive YSO candidates (either $J =$ "fill" or high reduced χ^2, indicating multiple or extended sources with large

TABLE 2

2MASS YOUNG STELLAR OBJECT AND T TAURI STAR CANDIDATES IN THE TRIFID NEBULA[a]

YSO Candidates				TTS Candidates			
Number	Designation	Number	Designation	Number	Designation	Number	Designation
1	2MASSI J1802121−230439	23	2MASSW J1802379−230211	1	2MASSI J1802158−230555	23	2MASSW J1802331−230135
2	2MASSI J1802211−230437	24	2MASSW J1802211−230234	2	2MASSI J1802102−230403	24	2MASSW J1802197−230136
3	2MASSI J1801592−230406	25	2MASSI J1802441−230245	3	2MASSI J1802129−230348	25	2MASSW J1802281−230142
4	2MASSW J1802139−230213	26	2MASSI J1802367−230302	4	2MASSW J1802197−230136	26	2MASSW J1802336−230154
5	2MASSW J1802142−230144	27	2MASSI J1802450−230332	5	2MASSI J1801575−230121	27	2MASSI J1802199−230305
6	2MASSI J1802168−230110	28	2MASSI J1802500−230334	6	2MASSI J1802124−225856	28	2MASSI J1802395−230343
7	2MASSI J1801561−230009	29	2MASSI J1802361−230428	7	2MASSI J1802173−225614	29	2MASSI J1802211−230437
8	2MASSI J1802044−225829	30	2MASSW J1802319−230440	8	2MASSI J1802108−225532	30	2MASSI J1802409−230459
9	2MASSI J1802122−225825	31	2MASSI J1802372−230503	9	2MASSI J1802205−225458	31	2MASSI J1802349−230505
10	2MASSW J1802202−225807	32	2MASSI J1802369−230656	10	2MASSI J1802205−225458	32	2MASSI J1802263−230730
11	2MASSI J1802401−225721	33	2MASSI J1802470−230702	11	2MASSI J1802162−225530	33	2MASSW J1802242−230910
12	2MASSI J1802377−225850	34	2MASSI J1802290−230704	12	2MASSI J1802464−225546	34	2MASSI J1802403−230913
13	2MASSI J1802463−225912	35	2MASSW J1802247−230729	13	2MASSI J1802473−225729	35	2MASSI J1802384−230934
14	2MASSI J1802433−225931	36	2MASSI J1802344−230806	14	2MASSI J1802367−225804	36	2MASSI J1803003−230134
15	2MASSI J1802491−225945	37	2MASSI J1802339−230924	15	2MASSW J1802312−225911	37	2MASSI J1802467−230130
16	2MASSI J1802503−225949	38	2MASSI J1802518−230810	16	2MASSW J1802305−225929	38	2MASSI J1802538−230033
17	2MASSI J1802438−225959	39	2MASSI J1802499−230740	17	2MASSW J1802228−225935	39	2MASSI J1802566−230026
18	2MASSI J1802441−230020	40	2MASSI J1802541−230736	18	2MASSI J1802175−225938	40	2MASSI J1803023−230022
19	2MASSI J1802266−230036	41	2MASSI J1802473−230428	19	2MASSI J1802409−225941	41	2MASSI J1802490−225656
20	2MASSW J1802226−230101	42	2MASSI J1802482−230309	20	2MASSI J1802344−230102		
21	2MASSI J1802467−230130	43	2MASSI J1802524−230227	21	2MASSI J1802284−230115		
22	2MASSW J1802271−230201	44	2MASSI J1802548−225901	22	2MASSW J1802408−230131		

[a] 2MASSI and 2MASSW indicate the Incremental Release and Working Database catalogs, respectively.

photometric uncertainties). These seven sources are likely protostars because their infrared colors are red and they also emit X-rays. By itself, an infrared color excess indicates either the presence of a YSO or a heavily extincted main-sequence star. The 2MASS counterparts of the X-ray sources are marked in the JHK_s color-color diagram (Fig. 3*a*) and on the 2MASS composite image (Fig. 3*d*). A few X-ray sources do not have obvious optical or 2MASS counterparts.

There are five known massive YSOs in the Trifid with mid-infrared emission detected using *ISO* (CLC98). These protostars were not identified as protostellar candidates from the 2MASS data, probably because they are too deeply embedded to be detected in the NIR. A 2MASS red star is the counterpart of the protostar TC2 in CLC98; we expect there are large numbers of such embedded protostars in the Trifid Nebula not detected in the NIR observations. This population is likely correlated with highly extincted dust lanes (see Fig. 3*d*) and molecular clouds.

4. X-RAY SPECTRAL ANALYSIS

The *ASCA* SIS image is shown in Figure 4 with the PSPC contours superposed. The X-ray emission is dominated by the emission from the O star. We extracted *ASCA* and *ROSAT* spectra from the entire region of the Trifid Nebula. The spectrum (Fig. 5*a*) shows clear Fe K line emission, along with weak Si and S lines, and a hard continuum tail up to 10 keV, the highest energy observable by *ASCA*. We extracted a background-corrected spectrum from a smaller region centered on HD 164492. HD 164492 is the brightest

TABLE 3

INFRARED COUNTERPARTS OF THE X-RAY SOURCES DETECTED IN PSPC IMAGES

RXT	2MASS[a] Counterparts	d[b] (arcsec)	R.A. (2000)[c]	Decl. (2000)[c]	J[d] (mag)	H[d] (mag)	K_s[d] (mag)	Comments[e]
RXT1.....	YSO	10	18 02 52.4	−23 02 27.2	15.17	13.93	13.18	...
RXT2.....	red	8	18 02 39.7	−22 58 29.0	17.72	15.06	13.50	J = "fill"
RXT3.....	red	5	18 02 41.4	−23 03 48.2	17.83	14.24	12.42	J = "fill"
	red	13	18 02 40.4	−23 03 58.9	15.58	12.37	10.90	High psf $\Delta\chi^2$
RXT4.....	red	12.8	18 02 36.8	−23 01 43.9	15.85	12.78	11.34	High psf $\Delta\chi^2$
RXT5.....	NONE	...	...	...	...	...	...	...
RXT6.....	TTS	13	18 02 30.5	−22 59 28.7	12.71	11.65	10.91	...
RXT7.....	YSO	12	18 02 26.6	−23 00 36.0	15.21	12.90	11.34	...
RXT8[f]	Multiple	...	...	...	...	...	...	...
RXT9.....	red	6	18 02 21.5	−23 03 19.0	15.04	13.58	11.87	J = "fill"
RXT10	NONE	...	...	...	...	...	...	...
RXT11[f].....	red	4	18 02 34.7	−22 59 52.1	16.52	12.42	10.58	J = "fill"
RXT12	red	9	18 02 31.3	−23 02 18.2	15.12	13.17	11.36	J = "fill"

NOTE.—Units of right ascension are hours, minutes, and seconds, and units of declination are degrees, arcminutes, and arcseconds.

[a] Notes for the 2MASS sources: TTS = T Tauri star; YSO = massive young stellar object; red = red 2MASS star.

[b] Projected distance between the X-ray and 2MASS sources.

[c] Coordinates of the 2MASS counterparts.

[d] J, H and K_s magnitudes of the 2MASS sources.

[e] J = "fill" means the J-band photometry is measured in band-filled within the aperture, indicating their photometric uncertainties are large. "High psf $\Delta\chi^2$" means the goodness of the fit of a point-spread function is high, indicating the sources are either extended or unresolved double sources.

[f] RXT8 is HD 164492 (O7 star) and/or YSO (TC1 in CLC98), and RXT11 also coincides with HD 313596 (B8 star).

X-ray source in the Trifid, and the shape of the spectrum of the entire region in the *ASCA* data is not significantly different from the spectrum of this star alone because of the broad *ASCA* point-spread function. We made hard (>3 keV) and soft (<3 keV) maps using the *ASCA* data, but no obvious difference was noticeable at the spatial resolution (1′) of *ASCA*. We also extracted an off-source *ASCA* spectrum in this direction, suspecting a contribution from the Galactic ridge emission. However, the off-source spectrum showed that the observed off-source emission is dominated by scattered emission from sources within the Trifid Nebula. The detection of hard emission from the Trifid is unusual because most single O stars have very little emission at energies above 2 keV and rarely show Fe K emission (Corcoran et al. 1993). The only massive stars to show such hard X-ray spectra are binaries, either high-mass X-ray binaries (HMXBs) with collapsed companions or colliding wind binaries with noncollapsed (O or W-R star) companions that have strong stellar winds and significant colliding wind X-ray emission.

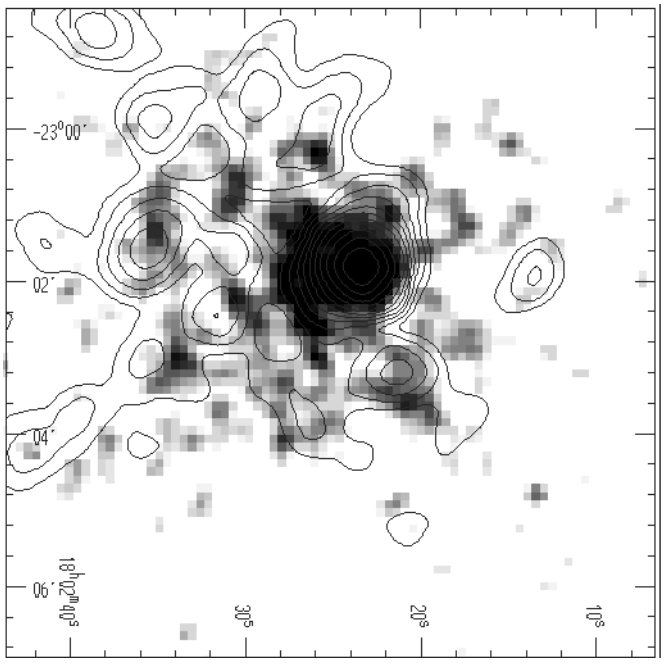

FIG. 4.—*ASCA* SIS image (gray scale ranges 0.7–4.5 counts (6.″4 pixel^{-1}) superposed on *ROSAT* contours.

We simultaneously fit the set of five spectra—the *ROSAT*/PSPC, *ASCA*/SIS0, SIS1, GIS2, and GIS3 spectra—using single- or two-temperature thermal models (Mewe-Kaastra plasma model; Kaastra 1992) with a single absorbing column density $N_{\rm H}$. The fits were unacceptable (reduced χ^2 of 3). We next attempted a two-temperature model. Following Corcoran et al.'s (1994) models of δ Ori and λ Ori, we also included an additional ionized ("warm") absorbing medium, as representative of the photoionized stellar wind material (Waldron 1984; Corcoran et al. 1994), and allowed different amounts of absorption for the hot and cold components. The line-of-sight extinction value is known toward this direction; $A_V = 1.3$–1.5 mag, i.e., $E(B-V) \sim 0.3$–0.4 mag (Kohoutek, Mayer, & Lorenz 1999; Lynds & O'Neil 1985). Using $E(B-V)$ of 0.4 mag, we expect an ISM $N_{\rm H}$ of $\sim 3 \times 10^{21}$ cm^{-2}, with which we have fixed the $N_{\rm H}$ value in our fit (also note that when we allow $N_{\rm H}$ to vary, 3×10^{21} cm^{-2} falls within the errors). The model yielded an acceptable fit with $kT_1 \sim 0.14$ keV (1.2×10^6 K) and $N_{\rm H,1} = 5.9 \times 10^{21}$ cm^{-2}, and a hotter component with $kT_2 \sim 3.3$ keV (3.9×10^7 K) and $N_{\rm H,2} = 2.7 \times 10^{21}$ cm^{-2}, with a line-of-sight ISM $N_{\rm H} = 3 \times 10^{21}$ cm^{-2}. The abundances are fixed at solar abundances. The fit results are summarized in Table 4, along with the Fe K line characteristics. The cold component arises from the O star atmosphere, but the hot component might arise from a number

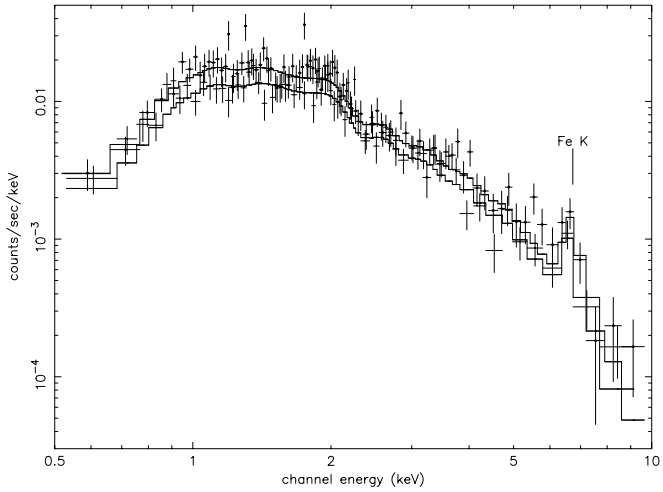

FIG. 5*a*

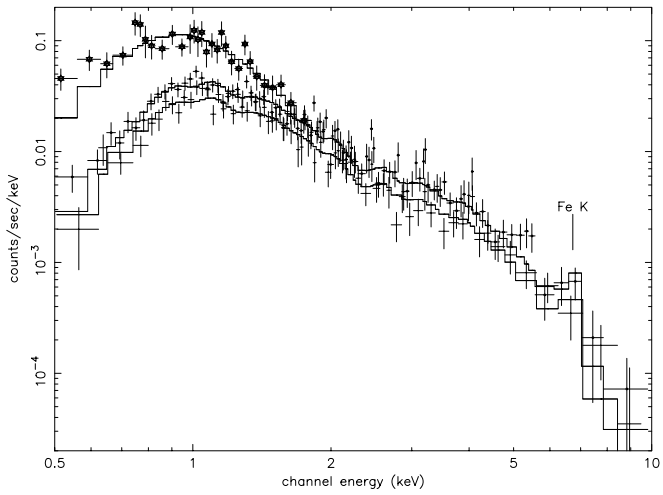

FIG. 5*b*

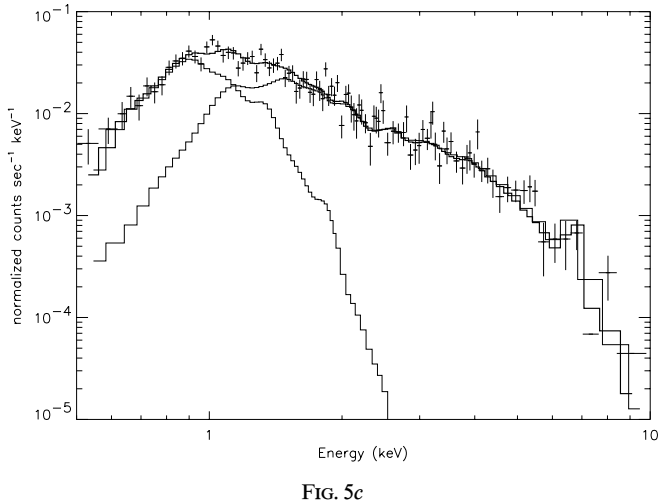

FIG. 5*c*

FIG. 5.—(*a*) GIS1 and GIS2 spectra of the Trifid Nebula with its best fit of a two-temperature thermal model with additional warm absorbing media. Hard emission and Fe XXV line appear in the spectra. (*b*) SIS0 and SIS1 and PSPC spectra with the best fits. (*c*) Each of two temperature components ($\sim 1.2 \times 10^6$ K and 3.9×10^7 K) is marked on the SIS0 spectrum.

of different sources, such as unresolved interacting binaries, active low-mass stars, or PMS stars.

5. THE NATURE OF THE HARD X-RAY COMPONENT

Our simultaneous *ASCA*/PSPC fits yield a total X-ray luminosity of 1.9–2.5 $\times$ 10^{34} ergs s^{-1} (0.3–10 keV) using the two-temperature model shown in Table 4. If attributed to HD 164492, then the ratio of X-ray and bolometric luminosities (= log L_X/L_{bol}) is between -5.0 and -4.5, which is much higher than the typical ratios of log $L_X/L_{bol} \sim -7$ for a single O-type star (Chlebowski & Harnden 1989; Berghöfer, Schmitt, & Cassinelli 1996). The 3 keV X-ray component is somewhat of a mystery since winds from single O-type stars are not known to produce such high-temperature emission. Typically the highest temperature emission observed in O star X-ray spectra has $kT < 1$ keV (e.g., Corcoran et al. 1994).

We discuss a few possibilities to explain the hot component in the Trifid Nebula. It may be that the hot component arises in the interaction of the wind from the O7.5 star with another object (either a companion star or a dense region of the nebula) outside the O star atmosphere. Colliding winds between an early-type star and an early-type companion (another O star or a Wolf-Rayet star) can produce shock-heated material in the wind interaction regions (Stevens, Blondin, & Pollock 1992), reaching temperatures of $10^7 - 10^8$ K, and emit X-rays. However, recent photometric and spectroscopic studies of this region found no evidence of a companion for HD 164492 (Kohoutek, Mayer, & Lorenz 1999). Unless the collision occurs far from the star ($d > 25''$), it will be unresolved to the *ROSAT* PSPC. However, recent radio and NIR observations toward the central region of the Trifid detected three sources close to the O star (Yusef-Zadeh et al. 2000), which may be either stars or nebular knots photoionized by the UV field of HD 164492.

Hard emission could also arise in single O stars from nonthermal emission produced by Fermi acceleration by shocks in the O star wind (Chen & White 1991). The hard component is suggested as a nonthermal tail produced by inverse Comptonization of the photospheric UV field by a population of fast particles accelerated by a distribution of shocks. Although it is not possible to determine if the hard emission is from a nonthermal tail or the two thermal temperature components from goodness of the fit to the spectra, the presence of the Fe K line suggests that the second component is thermal. The sources of the two spectral components need to be resolved spatially in order to determine their origins. Enhanced hard X-ray emission might also be produced by an oblique magnetic rotator, as is suspected in another O7 star, θ^1 Orionis C, the central star of the Orion Nebula (Gagné et al. 1997).

The X-ray properties of the core of the H II region W3 share a number of similarities to the Trifid emission. For W3, the luminosity is a few 10^{33} ergs s^{-1} with a similarly high temperature (Hofner & Churchwell 1997). In W3 (and possibly in the Trifid), the high-temperature component may be produced by a hot, wind-shocked cavity that results when strong stellar winds interact with a surrounding dense molecular cloud (e.g., Churchwell 1990). The presence of a known YSO (TC1 in CLC98) is consistent with the presence of a molecular cloud in the Trifid. In addition, *IRAS* observations of HD 164492 (van Buren, Noriega-Crespo, & Dgani 1995) show a bow-shock structure around the star,

TABLE 4

SPECTRAL FIT RESULTS FROM SIMULTANEOUS FIT USING *ASCA*/PSPC

Parameters	Trifid
ISM N_H (10^{21} cm^{-2})	$\equiv 3$
T_2	3.3 ± 0.6 keV ($= 3.9 \times 10^7$ K)
log EM$_2$(cm^{-3})	55.8
Wind N_H, hot component (10^{21} cm^{-2})	$2.7^{+2.3}_{-2.0}$
T_1	$0.14^{+0.06}_{-0.04}$ keV ($= 1.2 \times 10^6$ K)
log EM$_1$(cm^{-3})	57.4
Wind N_H, 1 component (10^{21} cm^{-2})	$5.9^{+1.1}_{-0.9}$
Flux	$2 \pm 0.5 \times 10^{-12}$
Unabsorbed flux	$8 \pm 2 \times 10^{-11}$
Luminosity (ergs s^{-1})	2.5×10^{34} [d(kpc)/(1.67 kpc)]^2
Fe K Line central energy (keV)	$6.65^{+0.1}_{-0.2}$
Fe K equivalent width (keV)	1.7 ± 0.3
Fe K flux (photons s^{-1} cm^{-2})	$6(\pm 0.4) \times 10^{-4}$

perhaps indicative of a wind-cloud collision that might produce the high-temperature X-ray emission. The stellar wind outflow at a speed of 1600 km s^{-1} should produce a postshock temperature of $\sim$30 million degrees, though the observed temperature may be lower since radiative cooling is rapid. CLC98 suggested that the HCO^+ molecular clouds (likely the dust lanes) are fragmented shell around the nebula. In other words, the clouds and dust lanes we see in the optical image are located at the surface of the ionized sphere. If this is the case, the 1600 km s^{-1} wind will be interacting with the lower density, ionized medium, and the shocked stellar wind can emit at high temperatures while the photoionized materials of the edge of clouds could supply sufficient density to emit strong X-rays.

The other possibility is that the hot component arises from deeply embedded young stars, especially since at least one embedded T Tauri star (TC1 in CLC98, which is marked in Fig. 1) exists near the O star. The TC1 source in CLC98 shows a large shift in the spectral energy distribution and violent ejections of high-velocity material (CLC98). Other *ASCA* observations showed bright X-ray sources with temperatures of 2–5 keV caused by flares of protostars in the ρ Ophiuchi dark cloud (Koyama et al. 1992), the Orion Nebula (Yamauchi & Koyama 1993), and the R Coronae Australis molecular cloud (Koyama et al. 1996). The hard emission was attributed to flares from individual PMS stars with typical X-ray luminosities in the range 10^{30}–10^{32} ergs s^{-1}, and the peak luminosity of flares is shown to be as large as 10^{33}–10^{35} ergs s^{-1} and a temperature as high as 10^8 K (Feigelson & Montmerle 1999; Grosso et al. 1997). The hard emission from W3 may be of a similar origin. Signs of active star formation in the Trifid have been reported recently (Lefloch et al. 2001): there is a dust cocoon or circumstellar disk around several members in the center of the Trifid, and one young stellar source shows a silicate feature in the circumstellar disk. Neither the ρ Ophiuchi dark cloud nor the R Coronae Australis molecular cloud is as bright in hard X-rays as the Trifid Nebula, which may imply there are a higher number of protostars present in the Trifid. A large number of protostars unresolved to *ASCA* would dilute any flux variability produced by flares.

In summary, one of two scenarios is likely responsible for the hard emission: The emission may arise from HD 169942 by the interaction of the wind from the O star with another object (a companion star or a dense region of the nebula) or from unresolved emission from active PMS stars. With our current data, we cannot determine if one is more favored than the other. To conclusively identify the hot component, a high-resolution image is needed to locate the emitting object to determine whether the observed emission is produced near the O star or whether a distributed group of active PMS stars dominates the observed emission. Along with the images, time-resolved spectra could allow us to distinguish whether the hard emission is flarelike (time variable).

6. IDENTIFICATION OF X-RAY AND INFRARED SOURCES WITHIN THE TRIFID

The detected X-ray sources and their counterparts are listed in Table 3. Most of X-ray sources are likely protostars or PMS stars; one source is a T Tauri star, two are massive protostars, and the others are unclassified protostars. The JHK_s color-color diagram using the 2MASS data suggests that there are $\sim$80 protostars present in this nebula. It has been shown already (CLC98; Lefloch & Cernicharo 2000) that massive protostars (17–60 $M_\odot$) are forming in the Trifid; they are associated with molecular gas condensations at the edges of clouds and their dynamical ages are less than 10^4 yr. Whether low-mass protostars and T Tauri stars can be formed in a young (3×10^5 yr) region such as the Trifid is still an open question. Low-mass PMS stars of similarly young age were found in the Orion Nebula using new *Chandra* observations (Hillenbrand et al. 1998; Garmire et al. 2000). The *Chandra* observation also showed the presence of young, low-mass (0.1–3 $M_\odot$) PMS stars as X-ray sources (Garmire et al. 2000). The populations of low-mass and massive protostars are similar in the Trifid, while we expect higher populations of low-mass protostars based on the initial mass function. This is consistent with the fact that the Trifid is a very young H II region; T Tauri stars have yet to form there. The distribution of T Tauri stars and massive YSOs is not obviously correlated with the molecular cloud distribution. It is possible that they are highly embedded in the molecular clouds, and their NIR colors cannot be fully obtained to identify protostars because either J and/or H flux is unavailable. This is consistent with the fact that 2MASS images show a higher population of red stars in the southern part of the Trifid. The *HST* images covering the southern part suggested the presence of embedded stars at the head of the evaporating globules (Hester et al. 1999). Deep NIR images and spec-

troscopy will likely reveal hundreds of young protostars in the Trifid as suggested by 2MASS and *HST* data.

Whether diffuse X-ray emission exists within the Trifid Nebula is currently unknown because of the limited spatial resolution of the PSPC images. For the unidentified X-ray sources 5 and 10, we cannot determine whether they are a part of diffuse emission or real point sources. They are very likely normal stars, but the possibility that they are knots of diffuse emission cannot be ruled out. Diffuse X-ray emission from H II regions has been detected, although it is rare. A few examples have been found, such as in the Carina Nebula (Seward & Chlebowski 1982), RCW 49 (Goldwurm, Caraveo, & Bignami 1987; Belloni & Mereghetti 1994), and the Cygnus Superbubble (Bochkarev & Sitnik 1985), and recently Wang (1999) reported diffuse X-ray emission from the giant H II region 30 Dor in the Large Magellanic Cloud. *ROSAT* and *Broadband X-Ray Telescope* observations of the Carina Nebula show large-scale diffuse emission over at least 40′, as well as discrete X-ray sources and hot gas surrounding η Car (Corcoran et al. 1995). The nature of diffuse emission is unclear in H II regions. Seward & Chlebowski (1982) suggested that stellar winds from the OB association adequately heat the plasma. Wang (1999) suggested that the X-ray thermal diffuse emission arises in blister-shaped region by loops of ionized gas and the structure is explained by the mass loading of the hot gas produced by the central OB association.

We compare the Trifid Nebula with 30 Dor to determine whether stellar winds in the Trifid may produce observable diffuse X-rays. The stellar wind luminosity in 30 Dor is a few $\times 10^{39}$ ergs s^{-1}, and the X-ray luminosity of 30 Dor is $\sim 10^{38}$ ergs s^{-1} (Wang 1999). The stellar wind luminosity of HD 146692 is $L_w = 1.7 \times 10^{36}(\dot{M}/2 \times 10^{-6}\ M_\odot\ \mathrm{yr}^{-1})(V/1580\ \mathrm{km\ s}^{-1})^2$ ergs s^{-1}. If the Trifid emits diffuse X-rays similarly to 30 Dor, we would expect $\sim 10^{35}$ ergs s^{-1} diffuse X-ray emission from the Trifid. This is higher than the total X-ray luminosity of the Trifid. It is likely that supernova heating contributes significantly to the bright X-ray emission from 30 Dor. The Trifid Nebula is too young to have hosted supernova explosions, so its diffuse X-ray emission should be much fainter than that of 30 Dor.

Future high-resolution X-ray observations by new telescopes such as *Chandra* and *XMM* should be able to resolve the O star from its immediate environment and discrete X-ray sources, such as T Tauri stars, numerous protostars, young and old normal stars, and to resolve the source of the high-temperature emission. A deep NIR image with other wavelength observations can identify the PMS stars and protostars and their mass populations. The Trifid Nebula is an exciting laboratory to understand the early stage of star-forming activities in H II region.

We thank Lynne Hillenbrand for helpful discussion on near-infrared colors of protostars and protostar disk models and for useful comments on the manuscript and John Carpenter for helpful discussion on 2MASS data. We thank Frank Winkler for allowing us to reproduce his optical image. For J. R., this work is partially supported by NASA/ADP grant, NASA-1407. This publication makes use of data products from the Two-Micron All-Sky Survey, which is a joint project of the University of Massachusetts and the Infrared Processing and Analysis Center, funded by the National Aeronautics and Space Administration and the National Science Foundation. J. R. and W. T. R. acknowledge the support of the Jet Propulsion Laboratory, California Institute of Technology, which is operated under contract with NASA.

REFERENCES

Alcalá, J. M., et al. 1995, A&AS, 114, 109
———. 1996, A&AS, 119, 7
Becker, R. H., White, R. L., Helfand, D. J., & Zoonematkermani, S. 1994, ApJS, 91, 347
Belloni, R., & Mereghetti, S. 1994, A&A, 286, 935
Berghöfer, T. W., Schmitt, J. H. M. M., & Cassinelli, J. P. 1996, A&AS, 118, 481
Bessell, M. S., & Brett, J. M. 1988, PASP, 100, 1134
Bochkarev, N. G., & Sitnik, T. G. 1985, Ap&SS, 108, 237
Casanova, S., Montmerle, T., Feigelson, E. D., & Andre, P. 1995, ApJ, 439, 752
Cernicharo, J., et al. 1998, Science, 282, 462 (CLC98)
Chen, W., & White, R. L. 1991, ApJ, 366, 512
Chlebowski, T., Harnden, F. R., Jr., & Sciortino, S. 1989, ApJ, 341, 427
Churchwell, E. 1990, A&A Rev., 2, 79
Conti, P. S., & Alschuler, W. R. 1971, ApJ, 170, 325
Corcoran, M. F., Swank, J., Rawley, G., Petre, R., Schmitt, J., & Day, C. 1995, Rev. Mexicana Astron. Astrofis. Ser. de Conf., 2, 97
Corcoran, M., et al. 1993, ApJ, 412, 792
———. 1994, ApJ, 436, L95
Feigelson, E. D., Casanova, S., Montmerle, T., & Guibert, J. 1993, ApJ, 416, 623
Feigelson, E. D., & Montmerle, T. 1999, ARA&A, 37, 363
Gagné, M., Caillault, J.-P., Stauffer, J. R., & Linsky, J. L. 1997, ApJ, 478, L87
Garmire, G., Feigelson, E. D., Broos, P., Hillenbrand, L. A., Pravdo, S. H., Townsley, L., & Tsuboi, Y. 2000, AJ, 120, 1426
Goldwurm, A., Caraveo, P. A., & Bignami, G. F. 1987, ApJ, 322, 349
Gregorio-Hetem, J., Montmerle, T., Casanova, S., & Feigelson, E. D. 1998, A&A, 331, 193
Grosso, N., et al. 1997, Nature, 387, 56
Hester, J. J., et al. 1999, BAAS, 194.681
Hillenbrand, L. A., et al. 1998, AJ, 116, 1816
Hofner, P., & Churchwell, E. 1997, ApJ, 486, L39
Howarth, I. D., & Prinja, R. K. 1989, ApJS, 69, 527
Kaastra, J. S. 1992, An X-Ray Spectral Code for Optically Thin Plasmas, SRON-Leiden Rept. (Leiden, Netherlands: SRON)
Kamata, Y., Koyama, K., Tsuboi, Y., & Yamauchi, S. 1997, PASJ, 49, 461
Kohoutek, L., Mayer, P., & Lorenz, R. 1999, A&AS, 134, 129
Koyama, K., Asaoka, I., Kuriyama, T., & Tawara, Y. 1992, PASJ, 44, L255
Koyama, K., Ueno, S., Kobayashi, N., & Feigelson, E. D. 1996, PASJ, 48, L87
Krautter, J., et al. 1997, A&AS, 123, 329
Lada, C. J., & Adams F. C. 1992, ApJ, 393, 278
Lefloch, B., & Cernicharo, J. 2000, ApJ, 545, 340
Lefloch, B., et al. 2001, A&A, 368, L13 (erratum 372, L65)
Levato, A. 1975, A&AS, 19, 91
Lynds, B. T., & O'Neil, E. J., Jr. 1985, ApJ, 294, 578
Meyer, M. R., Calvet, N., & Hillenbrand, L. 1997, AJ, 114, 288
Neuhäuser, R., Sterzik, M. F., Schmitt, J. H. M. M, Wichmann, R., & Krautter, J. 1995, A&A, 297, 391
Prinja, R. K., Barlow, M. J., & Howarth, I. D. 1990, ApJ, 361, 607
Rho, J.-H., Petre, R., Pisarski, R., & Jones, L. R. 1995, in Röntgenstrahlung from the Universe, ed. H.-U. Zimmermann et al. (Garching: MPE), 273
Rieke, G. H., & Lebofsky, M. J. 1985, ApJ, 288, 618
Seward, F. D., & Chlebowski, T. 1982, ApJ, 256, 530
Skrutskie, M. F., et al. 1997, in The Impact of Large-Scale Near-IR Sky Surveys, ed. F. Garzon, N. Epchtein, A. Omont, B. Burton, & P. Persi (Dordrecht: Kluwer), 25
Stevens, I. R., Blondin, J. M., & Pollock, A. M. 1992, ApJ, 386, 265
Tanaka, Y., Inoue, H., & Holt, S. S. 1994, PASJ, 46, L37 (TI of H94)
Trümper, J. 1993, Science, 260, 1769
van Buren, D., Noriega-Crespo, A., & Dgani, R. 1995, AJ, 110, 2914
Waldron, W. L. 1984, ApJ, 282, 256
Wang, Q. D. 1999, ApJ, 510, L139
Wichmann, R., Sterzik, M., Krautter, J., Metanomski, A., & Voges, W. 1997, A&A, 326, 211
Yamauchi, S., & Koyama, K. 1993, ApJ, 405, 268
Yusef-Zadeh, F., Shure, M., Wardle, M., & Kassim, N. 2000, ApJ, 540, 842